1   # In situ Raman spectroscopy identification of the S_3^- ion in S-

2   # rich hydrothermal fluids from synthetic fluid inclusions

3

4   Nicolas Jacquemet[1,*], Damien Guillaume[1], Antoine Zwick[2], and Gleb S.

5   Pokrovski[1]

6

7   [1]Géosciences Environnement Toulouse (GET, UMR 5563), CNRS, Université de Toulouse, IRD,

8   14, avenue Edouard Belin, F-31400, Toulouse, France

9   [2]Centre d'Elaboration de Matériaux et d'Etudes Structurales CEMES-CNRS-Université de

10   Toulouse, 29 rue Jeanne Marvig, F-31055 Toulouse, France

11

12   *E-mail: nicolas.jacquemet@get.obs-mip.fr, nicolas_jacquemet@yahoo.fr

13

14   # Revision 1

15   # Manuscript #4524R

16

17

18   *American Mineralogist, November 2013*

19

1

Manuscript #4524R, Revision 1

20   **ABSTRACT**

21   The chemical forms of sulfur in geological fluids control the behavior of this element and

22   associated base and precious metals in magmatic, hydrothermal, and metamorphic environments.

23   However, these forms are insufficiently known at elevated temperature (T) and pressure (P). In

24   this study, sulfur speciation in model aqueous solutions of thiosulfate and sulfur (~3 wt% of total

25   S) was examined by in situ Raman spectroscopy on synthetic fluid inclusions at T-P-pH-redox

26   conditions typical of porphyry Cu-Au-Mo deposits. Fluid inclusions were entrapped at 2 kbar and

27   600 or 700°C in quartz that served as a container for the high T-P fluid. Then, the inclusion-

28   bearing quartz samples were re-heated and examined by Raman spectroscopy as a function of T

29   and P (up to 500°C and ~1 kbar). At $T < 200$°C, all fluid inclusions show sulfate ($SO_4^{2-} \pm HSO_4^-$)

30   and sulfide ($H_2S \pm HS^-$) in the aqueous liquid phase and elemental sulfur (S_8) in the solid/molten

31   phase; these results agree both with thermodynamic predictions of sulfur speciation and the

32   common observation of these three S forms in natural fluid inclusions. At $T \geq 200$-300°C, in

33   addition to these S species, the S_3^- ion was found to appear and grow with increasing temperature

34   to at least 500°C. The formation of S_3^- is rapid and fully reversible; its Raman signal disappears

35   on cooling below 200°C, and re-appears on heating. These new data confirm the recent findings

36   of S_3^- in similar aqueous solutions at P of 5-50 kbar and $T \geq 250$°C; they suggest that S_3^- may

37   account for some part of dissolved sulfur and serve as a ligand for chalcophile metals in fluids

38   from subduction zones and related Cu-Au-Mo deposits. This work demonstrates that in situ

39   approaches are required for determining the true sulfur speciation in crustal fluids; it should

40   encourage future spectroscopic investigations of natural fluid and melt inclusions at high

41   temperatures and pressures close to their formation conditions.

42   **Keywords:** Hydrothermal fluid, Raman spectroscopy, sulfur, sulfate, sulfide, trisulfur ion,

43   fluid inclusion

INTRODUCTION

44

45   The concentration and chemical forms of sulfur in hydrothermal fluids are controlling

46   factors of metal transport and deposition as sulfide ores in magmatic-hydrothermal environments

47   (e.g., Simon and Ripley 2011; Kouzmanov and Pokrovski 2012; references therein). The widely

48   accepted model of sulfur speciation in crustal fluids at elevated temperatures is that sulfate,

49   sulfide, and sulfur dioxide (the latter mostly in gas phase) are the major S species (Barnes 1979;

50   Hedenquist and Lowenstern 1994; Seward and Barnes 1997). However, this model is largely

51   based on studies of samples brought to the Earth's surface and analyzed at near-ambient

52   conditions, such as ores, silicate glasses, volcanic sublimates or fluid inclusions in minerals.

53   Little attention has been given in previous work to the fact that sulfur chemistry and solubility in

54   the fluid phase is very sensitive to temperature (T), pressure (P), redox, and acidity (pH)

55   conditions (e.g., Simon and Ripley 2011). Thus, the major weakness in our knowledge of sulfur

56   in deep and hot geological fluids is the lack of in situ approaches for studying such systems. The

57   dominant presence of sulfide and sulfate in hydrothermal fluids has recently been challenged by

58   Pokrovski and Dubrovinsky (2011) who used in situ Raman spectroscopy in a diamond-anvil cell

59   to show that, in addition to those two 'classical' S species, the hypersulfide (or trisulfur) ion, S_3^-,

60   may be stable in S-rich aqueous solution at T from ~300 to at least 450°C and P from 5 to 50

61   kbar, corresponding to fluids from deep and cold domains of subduction zones. However, it

62   remains uncertain to which extent S_3^-, and other intermediate-valence S species, may form in less

63   deep fluids responsible for the formation of most metal ore deposits in the crust (P < 1-2 kbar,

64   depth ≤ 5 km).

65   The only direct witnesses of these fluids are fluid inclusions trapped by minerals during

66   their growth or later deformation. Quantitative analyses of total sulfur concentrations in natural

67   fluid inclusions were performed on inclusion populations by crush-leach methods (e.g., Banks

3

68   and Yardley 1992; Bray and Spooner 1992) or on individual inclusions by proton-induced X-ray

69   emission (Ryan et al. 1993), synchrotron X-ray fluorescence (Cauzid et al. 2007), and recently

70   laser ablation-inductively coupled plasma-mass spectrometry (Guillong et al. 2008; Seo et al.

71   2009; Catchpole et al. 2011, 2012). However, all these methods analyze bulk sulfur contents and

72   cannot assess sulfur redox and speciation which require in situ spectroscopic techniques. Among

73   them, Raman spectroscopy is the best suited, and was used for identifying sulfur species both in

74   natural (e.g., Rosasco and Roedder 1979; Bény et al. 1982; Boiron et al. 1999; Giuliani et al.

75   2003) and synthetic (e.g., Binder and Keppler 2011) fluid inclusions at ambient temperature. To

76   the best of our knowledge, the only studies at elevated temperatures are those of Jacquemet et al.

77   (2005, 2012) and Pironon et al. (2007) who performed Raman spectroscopy analyzes on H_2S-

78   bearing fluid inclusions up to 200°C. The sulfur species detected in all these studies are sulfate

79   (SO_4^{2-}), hydrogen sulfate (HSO_4^-), sulfur dioxide (SO_2), hydrogen sulfide (H_2S, HS^-), and

80   elemental sulfur (S^0).

81   The present study is aimed at investigating sulfur speciation in model aqueous S-bearing

82   fluids at *T-P* conditions typical of hydrothermal-magmatic ore formation. For this purpose,

83   synthetic fluid inclusions of such fluids were probed by in situ micro Raman spectroscopy to

84   500°C and 1 kbar. Results show that sulfur speciation at elevated *T-P* is different from what may

85   be expected from low-temperature observations; they highlight the importance of in situ

86   approaches for studying geological fluids.

87

88   **MATERIALS AND METHODS**

89   **Experimental strategy and samples**

90   Three model aqueous S-bearing solutions similar to those studied by Pokrovski and

91   Dubrovinsky (2011), prepared from deionized degassed water and analytical-grade chemicals,

4

92   were investigated (Table 1): 1) thiosulfate ($K_2S_2O_3$-$Na_2S_2O_3$, hereafter named as Thios); 2)

93   thiosulfate + HCl ($K_2S_2O_3$-$Na_2S_2O_3$-HCl, Thios-HCl) and 3) elemental sulfur + NaOH (S-

94   NaOH). The total sulfur concentration in these solutions is about 3 wt%, which is comparable to

95   that recently measured in fluid inclusions from porphyry Cu-Au-Mo deposits (Seo et al. 2009,

96   2012). The three model solutions were entrapped as fluid inclusions in quartz at 2 kbar and

97   600°C (Thios and Thios-HCl experiments) or 700°C (S-NaOH experiment). These *T-P*

98   conditions correspond to early stages of the magmatic-hydrothermal evolution of porphyry

99   deposits (e.g., Sillitoe 2010; Kouzmanov and Pokrovski 2012). The quartz crystals hosting

100   inclusions were then examined on a heating stage by Raman micro spectroscopy from ambient

101   temperature to 400 or 500°C (depending on the system, Table 1), covering the typical

102   temperature range of hydrothermal ore deposit formation.

103   The chemical systems chosen in this study represent a good proxy for natural S-rich fluids

104   in arc-related magmatic-hydrothermal systems, which are characterized by acidic-to-neutral pH

105   and redox conditions close to that of the hematite-magnetite mineral buffer (Einaudi et al. 2003;

106   Kouzmanov and Pokrovski 2012). Redox and acidity buffering in our experiments is achieved

107   through the sulfide-sulfate and sulfate-hydrogensulfate exchange reactions, respectively (see

108   below). These species are produced by breakdown of thiosulfate and dissolution of sulfur at

109   elevated temperatures as shown by many previous experiments in hydrothermal reactors (e.g.,

110   Ohmoto and Lasaga 1982; Uyama et al. 1985; Pokrovski et al. 2008; references therein) and

111   thermodynamic calculations below. Because redox reactions between sulfate and sulfide in

112   aqueous solution are rather slow at moderate temperatures (Ohmoto and Lasaga, 1982), complete

113   equilibrium is likely to be not attained in our runs below 200-250°C. Nevertheless, even at such

114   moderate *T*, redox potential is controlled by the sulfate/sulfide ratio, which is almost constant,

115   being imposed by the stoichiometry of decomposed thiosulfate (see below). The sulfate-sulfide

116   exchange rates rapidly increase with increasing T (Ohmoto and Lasaga, 1982), all our runs at $T >$

117   300°C are likely to be close to equilibrium. In addition, as found by Pokrovski and Dubrovinsky

118   (2011) for similar systems at higher pressures, the presence of polysulfide species in our

119   concentrated solutions might further accelerate sulfate-sulfide exchange compared to dilute

120   solutions studied so far (Ohmoto and Lasaga, 1982). Note also that in contrast to redox reactions

121   which require electron transfers, protonation and ion pairing in aqueous solution are usually very

122   fast processes, so that equilibrium among such species (e.g., SO_4^{2-}, HSO_4^-, $NaSO_4^-$) is achieved at

123   any temperature within the run duration.

124   The calculated equilibrium distribution of dominant sulfur species in the three

125   experimental systems at the T-P conditions of the fluid entrapment and Raman spectroscopy

126   analyses is shown in Figure 1. These calculations were performed using the available

127   thermodynamic properties of aqueous and solid sulfur species from reference databases

128   (SUPCRT, JANAF) with minor modifications (see Supplementary Table 1, and Pokrovski et al.

129   2009 for details), and the HCh computer code (Shvarov 2008). The activity coefficients were

130   approximated using the extended Debye-Hückel equation for charged species and assumed to be

131   unity for neutral species; these models are widely adopted in calculations of hydrothermal fluid-

132   mineral equilibria (Helgeson et al. 1981; Oelkers et al. 2009; references therein). Note that

133   variations of different model parameters (e.g., electrostatic radius, extended Debye-Hückel term)

134   yield insignificant changes in calculated species fractions owing to: a) partial cancellation of

135   activity coefficients in reactions involving similarly charged species as reagents and products

136   (e.g., reaction 1 below), and b) sulfur redox balance imposed by the decomposition of thiosulfate

137   and sulfur.

138   In the thiosulfate system at near-neutral pH ($5.4 \leq$ pH ≤ 7.5, depending on T and P), the

139   calculated distribution of sulfur species above 200°C corresponds to an overall sulfide-to-sulfate

Manuscript #4524R, Revision 1

140   ratio of 1 (Fig. 1), as imposed by redox balance according to the thiosulfate disproportionation

141   reaction:

142   $S_2O_3^{2-} + H_2O = SO_4^{2-} + H_2S$ (1)

143   The formation of alkali ion pairs ($NaSO_4^-$, KSO_4^-), partial dissociation of H_2S to HS^-, and sulfate

144   protonation yielding minor amounts of HSO_4^- (Fig. 1) are added to this reaction. At $T < 300°C$, a

145   part of sulfur remains undissolved in the form of solid or molten elemental sulfur due to its low

146   solubility at such temperatures. At more acidic pH ($1.2 < pH < 5.5$) in the Thios-HCl system

147   below 400°C, a significant fraction of sulfur is in the elemental form; it dissolves with increasing

148   temperature, accompanied by an increase of the amount of H_2S and HSO_4^-, which are the

149   dominant species to 600°C (Fig. 1). Above 400°C, SO_2 is added to these species with fractions

150   increasing with T and reaching ~ 20% of the total dissolved S at 600°C (Fig. 1). In the S-NaOH

151   system ($5.1 < pH < 7.5$), the redox balance imposes a sulfide-to-sulfate ratio of ~3 in solution at

152   all temperatures (Fig. 1), according to the disproportionation reaction of sulfur in water at near-

153   neutral pH:

154   $4\ S + 4\ H_2O = 3\ H_2S + SO_4^{2-} + 2\ H^+$ (2)

155   Above 300°C molten sulfur dissolves, and above 400°C SO_2 appears in the system with fractions

156   less than 10% of the total dissolved sulfur.

157   The advantage of using these model systems is that they provide oxygen fugacity (f_{O2})

158   and acidity buffering via the reactions:

159   $H_2S + 2\ O_2 = SO_4^{2-} + 2\ H^+$ (3)

160   $SO_4^{2-} + H^+ = HSO_4^-$ (4)

161   yielding f_{O_2} values close to the hematite-magnetite buffer and pH values from 1.2 to 7.5

162   corresponding to the acidic-to-neutral region (pH of the neutrality point of pure water at our T-P

7

163   conditions is between 5.4 and 7.3). As a result, reactions (1) to (4) impose robust chemical

164   constraints (redox balance, f_{O_2} and pH) on the experimental systems independently of possible

165   presence of low-to-moderate amounts of other S species (Pokrovski et al. 2009; Pokrovski and

166   Dubrovinsky 2011).

167

168   **Preparation of synthetic fluid inclusions**

169   Fluid inclusion syntheses were conducted following a procedure inspired from Sterner

170   and Bodnar (1984) and widely adopted in more recent studies (e.g., Lamb et al. 1996; Gibert et

171   al. 1998; Duc-Tin et al. 2007; Ulrich and Mavrogenes 2008; Zajacz et al. 2010, 2011; Frank et al.

172   2011; Zhang et al. 2012). Prefractured quartz lamellas were used to trap the fluid inclusions at T-

173   P of the experiments. Quartz lamellas of ~5×2×1.5 mm size were prepared from inclusion-free

174   natural crystals sampled at Kerguelen Island. The lamellas were heated at 700°C for 15 min,

175   quenched in water to produce micro-fractures and dried at 700°C to evaporate the capillary water

176   from the micro-fractures. Gold capsules (40 mm length, 4 mm outside diameter, 0.2 mm wall

177   thickness) were loaded with 80 - 110 µL of aqueous solution and several quartz lamellas, then

178   sealed using an electric arc. Sealing was checked by weighing the capsules after they were heated

179   at 90°C for one hour.

180   The capsules were put in a cold-seal hydrothermal vessel placed in a horizontal furnace

181   and connected to a hydraulic pressure line in a configuration similar to that of Gibert et al.

182   (1998). The vessel was pressurized to 10-20 bar at ambient T, then heated to 600 or 700°C during

183   ~1.5 hour. The thermal gradients were ~10°C over the length of the capsule. The final pressure

184   was adjusted to 2 kbar using the pressure line. After 6-17 days at the experimental T-P, the

185   reactor was cooled down in air stream, reaching $T < 100$°C in less than 10 min. The gold capsules

8

186   were weighed to check for eventual leaks, punctured to release H_2S (gas), and opened to recover

187   the quartz lamellas, which were double-polished for microscopy analyses. The fluid inclusion

188   homogenization temperatures (T_h) were measured by microthermometry at the GET laboratory on

189   a Linkam THMSG-600 heating-freezing stage connected to the microscope and a programmable

190   thermal control unit. The stage was calibrated with pure CO_2 fluid inclusions in quartz from

191   Camperio, Central Alps (Mullis et al. 1994; Poty and Stadler 1974) at the CO_2 triple (-56.6°C)

192   and critical (+31.1°C) point temperatures and synthetic H_2O fluid inclusions in quartz at the H_2O

193   triple (+0.2°C) and critical (375.13°C) point temperatures.

194

Raman spectra acquisition and analysis

196   Spectra were recorded at the CEMES laboratory (Toulouse, France) with a Jobin Yvon

197   Horiba Xplora spectrometer in a back-scattering geometry and using a 532.1 (green) or 637.7 nm

198   (red) solid-state laser as the excitation source (~1-2 μm spot size on the sample). The use of

199   multiple excitation wavelengths allows for more robust identification of certain sulfur species,

200   particularly those exhibiting Raman resonance phenomena, because their Raman peak intensities

201   strongly vary as a function of laser frequency (e.g., Clark and Franks 1975; Clark and Cobbold

202   1978).

203   The acquisition was performed using an Olympus BX 5 microscope equipped with a

204   Linkam heating-freezing stage and a dark-field long-working distance (10.5 mm) ×50 objective,

205   in the 35-5042 cm^{-1} spectral window with a grating of 600 lines/mm, an entrance slit of 100 or

206   200 μm, and a confocal hole of 100 μm; spectral resolution was ~5-10 cm^{-1} and acquisition times

207   varied from 7 to 60 seconds (depending on the signal intensity). The maximal laser power at the

208   sample is ~15 mW. Some spectra were also acquired at lower laser power; they were compared

Manuscript #4524R, Revision 1

209 with the full power spectra to check for eventual laser-induced phenomena (see below). The

210 spectrometer was calibrated before and after each analytical session using the well-known Raman

211 stretching vibrations of pure silicon (520.6 cm^{-1} at 20°C), and oxygen (1555 cm^{-1}) and nitrogen

212 (2331 cm^{-1}) gas from the air. In addition, certain sharp Raman bands of our quartz samples

213 themselves (e.g., 464 cm^{-1}, see below) provide a complementary check for the energy position

214 during a Raman session.

215   The microscope heating-freezing stage allowed the quartz chips to be re-heated and the

216 different phases in fluid inclusions (solid, liquid, vapor, and supercritical fluid) to be probed at

217 25, 200, 300, and 400°C (and 500°C for the S-NaOH run). Higher temperatures could not be

218 reached because of the inclusion's decrepitation due to the elevated internal pressure. The

219 pressure inside the fluid inclusions containing vapor and liquid phases at $T \leq 300$°C corresponds

220 to the saturated vapor pressure of the system, which is likely to be slightly higher than the vapor

221 pressure of pure water or a water-salt solution due to partitioning of H_2S into the vapor phase (see

222 Table 1). All inclusions homogenize to liquid at 350-360°C (see below); above that temperature,

223 the pressure was estimated using linear isochores connecting the homogenization point with the

224 fluid entrapment point in P-T space (Fig. 2).

225   Raman spectra were processed using the Fityk software (Wojdyr 2010). A baseline,

226 closely matching that of the host quartz spectrum recorded near the fluid inclusion was subtracted

227 from the fluid inclusion spectrum. To determine their frequency position and area (or integrated

228 intensity), Raman peaks were fitted with a set of pseudo-Voigt functions, which are a linear

229 combination of a Lorentzian (L) and a Gaussian (G), with the L/G ratio varied between 0 (pure

230 Gaussian) and 1 (pure Lorentzian) to account for the wide range of band widths and profiles

231 depending on the species nature. This type of function was chosen for the sake of consistency

232 with the previous studies of S species in aqueous solution (e.g., Schmidt 2009; Pokrovski and

10

Manuscript #4524R, Revision 1

233   Dubrovinsky 2011; Pokrovski and Dubessy 2012); the results being insensitive to the exact

234   function choice within fit uncertainties. Raman peak absolute areas are strongly dependent on the

235   ensemble of acquisition parameters discussed above and the inclusion size and depth, so that

236   normalization is required to be able to compare data for different temperatures and experiments.

237   The only possible 'internal standard' in our experimental systems is water whose O-H stretching

238   band between 2800 and 3800 cm^{-1} is little sensitive to the solute composition in the experimental

239   water-dominated liquid-like solutions. The water band integrated intensity is a direct and smooth

240   function of temperature and fluid density (e.g., Frantz et al. 1993); it was found to change

241   relatively little in our T-P-density range. In the liquid phase, the O-H peaks area decreases by

242   only a factor of two from ambient temperature to the homogenization point (~350°C, see below),

243   then remains almost constant in the supercritical region at constant density (~0.7 g/cm^3).

244   Consequently, when determining the peak areas of sulfur species, the spectra of the liquid and

245   supercritical phase were normalized to this band; this allowed a quantitative comparison of their

246   intensities at the same temperature in different experiments. The Raman frequencies and

247   normalized areas of major species bands in the liquid and supercritical phase are reported in

248   Supplementary Table 2. The overall uncertainties of peak areas are between 10 and 30 % of the

249   value depending of the signal intensity.

250

251   **RESULTS**

252   **Phase composition and relationships in the fluid inclusions**

253   Optical microscopy and microthermometry show that all inclusions from the three

254   experiments contain aqueous liquid and vapor at $T \leq 300°C$ (Fig. 3a-3c). In addition to these

255   phases, solid and molten (above ~115°C) elemental sulfur is detected in the Thios-HCl and S-

256   NaOH experiments (Fig. 3b and 3c; see below for its Raman identification). Sulfur spheres were

Manuscript #4524R, Revision 1

257   also identified on the surface of the recovered quartz lamellas and internal walls of the capsule at

258   ambient conditions after these experiments by optical and scanning electron microscopy

259   (Supplementary Fig. 1). The occurrence of elemental sulfur agrees with thermodynamic

260   predictions of its solubility (Fig. 1).

261   All inclusions homogenize in a narrow temperature range, with the mean homogenization

262   temperatures (T_h) values of 350±2, 352±2, and 360±3°C (± standard deviation) for the Thios,

263   Thios-HCl, and S-NaOH runs as based on 6, 12, and 11 data points, respectively. These T_h values

264   are consistent with the calculated density of the fluids at experimental T-P (0.70±0.07 g/cm^3 in

265   Thios and Thios-HCl runs, and 0.60±0.06 g/cm^3 in S-NaOH runs), assuming that they may be

266   approximated by equivalent NaCl-H_2O solutions of same weight concentration and using the

267   SoWat software (Driesner and Heinrich 2007). Such an approximation is more reliable than that

268   by pure water, because the experimental solutions contained Na$^+$ and anions similar to Cl$^-$ (SO$_4^{2-}$,

269   OH$^-$, HSO$_4^-$); its expected uncertainty should not exceed 10 % of the density value in the

270   experimental T-P range (e.g., Pokrovski et al. 2009). The density and T_h values strongly suggest

271   that all inclusions in each of the three experiments belong to a single population trapped at the

272   experimental T-P (600 or 700°C at 2 kbar).

273

Raman spectra of the host quartz

275   Raman spectra of the host quartz at ambient conditions (Supplementary Fig. 2) are

276   characterized by three major peaks at 132, 208 and 469 cm^{-1}, and a number of minor peaks (

277   ~270, 360, 400, 700, 810, 1160 cm^{-1}). This pattern is in good agreement with the well-

278   documented Raman spectra of the main peak positions of α-quartz (~130, ~210, and 464-467 cm$^-$

279   ^{1} at ambient conditions; RRUFF database at http://rruff.info/). With increasing temperature, most

12

280 bands exhibit a small ($\sim$3-5 cm^{-1}) shift towards lower frequencies, and the relative intensities of

281 the low-frequency bands (< 300 cm^{-1}) increase with increasing T, consistent with the reported

282 temperature dependence of quartz Raman spectra (e.g., Shapiro et al., 1967). The largest changes

283 are observed for the $\sim$210 cm^{-1} band that exhibits a significant low-energy shift and increasing

284 broadening with temperature, due to changes in the α-quartz network when approaching the $\alpha-\beta$

285 transition ($\sim$573°C, Shapiro et al. 1967).

286

287 **Raman spectra of the vapor and solid phases**

288   The detectable gas species in the vapor phase of all inclusions below T_h are H_2S and H_2O

289 (Fig. 4a), unambiguously identified by their well-known symmetric stretching vibration mode

290 frequencies at respectively 2607-2612 cm^{-1}, and 3630-3660 cm^{-1}, depending on temperature and

291 pressure (Frantz et al. 1993; Burke 2001; Frezzotti et al. 2012). In addition, H_2 (gas) was found in

292 the Thios experiment at 300°C (4156 cm^{-1}, Burke 2001). The solid phase in the Thios-HCl and S-

293 NaOH experiments gives three main peaks at $\sim$153, $\sim$221 and $\sim$469 cm^{-1} (Fig. 4b), which belong

294 to the S_8 solid or molten elemental sulfur (Pasteris 2001; Giuliani et al. 2003; Frezzotti et al.

295 2012). Note that although the main stretching vibration of S_8 (462-474 cm^{-1} in different studies)

296 is very close to that of SiO_2 ($\sim$464 cm^{-1}), it cannot come from the host quartz because the other

297 main quartz peaks ($\sim$130 and $\sim$210 cm^{-1}, see above) showing no overlap with the S_8 spectrum are

298 very minor in the sulfur spectrum of Figure 4b. The S_8 molecule corresponds to the

299 thermodynamically stable sulfur allotrope at these conditions (Steudel 2003).

300

301 **Raman spectra of the liquid and supercritical fluid phases**

13

Manuscript #4524R, Revision 1

302   In the three systems, the Raman spectra of the liquid phase are dominated by the broad

303   asymmetric band of H_2O around 3400 cm^{-1} at ambient conditions. As the temperature increases,

304   the intensity of the low-frequency side of the band decreases while the high-frequency side is

305   shifted towards greater frequencies. The band shape and its evolution with temperature are in

306   agreement with those described in detail in previous Raman studies of pure water; they mostly

307   reflect changes in hydrogen bonding (e.g., Frantz et al. 1993; references therein). No detectable

308   differences in the shape and evolution of the H_2O band were found among the three experiments,

309   which is consistent with the low solute concentrations relative to that of H_2O (e.g., Dubessy et al.

310   2002).

311   Among the solute species, SO_4^{2-} is identified in the three systems according to its

312   characteristic S-O_4 symmetric stretching vibration between 970 and 980 cm^{-1} (depending on

313   temperature; Dubessy et al. 1992; Schmidt 2009). Note that the spectral resolution does not allow

314   sulfate-alkali ion pairs to be distinguished from the free SO_4^{2-} ion. Thus this band represents the

315   whole sulfate form composed of thermodynamically distinct aqueous species (Supplementary

316   Table 1). Sulfate is visible in the whole temperature range covered by measurements (25-400°C)

317   in the Thios and Thios-HCl systems, and from 25 to 300°C in the S-NaOH system (Fig. 5a-5c).

318   The sulfate peak intensity is highest in the Thios system at near-neutral pH; it decreases with

319   increasing temperature and decreasing pH (*cf.* Thios versus Thios-HCl). This evolution is in

320   agreement with the thermodynamic calculations predicting the increasing protonation of SO_4^{2-} to

321   form the hydrogensulfate ion (HSO_4^-) at acidic pH and elevated *T* (Fig. 1). The latter species,

322   with a stretching vibration at ~1050 cm^{-1} (Dubessy et al. 1992; Rudolph 1996), is identified in the

323   Thios-HCl experiment at 200°C (Fig. 5b), but at higher *T* its characteristic Raman peak is hidden

324   within a quartz band and the far more intense second-order overtone of the S_3^- band (see below).

14

325   Aqueous hydrogen sulfide (H_2S), having an $S-H_2$ stretching vibration at $\sim$2590 cm^{-1} (e.g.,

326   Dubessy et al. 1992) is clearly visible in the three systems in the whole T range covered by

327   measurements (Fig. 5a-5c). In addition, its ionic counterpart (HS^-) with an S-H stretching

328   vibration at $\sim$2570 cm^{-1} (Meyer et al. 1983) is identified in the Thios system from 25 to 200°C,

329   but disappears in favor of H_2S at higher T (Fig. 5a), in agreement with thermodynamic

330   predictions (Fig. 1).

331   No thiosulfate ions ($S_2O_3^{2-}$), which have a narrow SO_3 stretching band at $\sim$ 1000 cm^{-1}

332   easily distinguishable from sulfate (Meyer et al. 1980), and an intense S-S stretching band at

333      $\sim$450 cm^{-1}, which should appear at the low-frequency side of the 464 cm^{-1} band of quartz, were

334   detected in the solutions. The absence of thiosulfate is consistent with its irreversible breakdown

335   at temperatures above 200°C (e.g., Pryor 1960; Pokrovski and Dubrovinsky 2011). No sulfur

336   dioxide (SO_2, $\sim$1150 cm^{-1}, Ni and Keppler 2012; references therein) was observed probably both

337   due to its small amounts at T < 400-500°C (Fig. 1) and the overlap of its characteristic peak with

338   those of quartz. No polysulfide ions (S_nS^{2-}), characterized by multiple S-S stretching vibrations

339   between 350 and 480 cm^{-1} (e.g., Steudel 2003; Tsujimura et al. 2004; references therein) were

340   detected likely owing to their minor amounts ($\leq$ 10% of total sulfur) as predicted by

341   thermodynamics at T < 200°C (Fig. 1) and overlaps with the intense quartz bands that dominate

342   the Raman low frequencies (< 500 cm^{-1}).

343   The most remarkable feature of the Raman spectra in the three experiments above 200°C

344   is the growth of the trisulfur ion (S_3^-), which is unambiguously identified by its characteristic

345   resonance spectrum consisting of the enhanced symmetric S-S stretching vibration (ν) at $\sim$530-

346   540 cm^{-1} and its higher-order overtones 2ν, 3ν, 4ν, and 5ν at $\sim$1070, $\sim$1600, $\sim$2130, and $\sim$2650

347   cm^{-1}, respectively (Fig. 5a-5c). This particular Raman pattern is due to a resonance phenomenon

15

Manuscript #4524R, Revision 1

348   favored by the enhanced absorption of the laser light by this blue species at the laser wavelengths

349   used (see Pokrovski and Dubrovinsky 2011 for details and references). The Raman pattern of S_3^-

350   is unique and cannot be mixed up with that of any other sulfur species (Chivers and Drummond

351   1972; Chivers and Elder 2013; references therein). The S-S bending vibration (δ) of S_3^- at ~220

352   cm^{-1} and resonance-induced combinatory bending-stretching overtones (e.g., $\nu+\delta$, $\nu-\delta$, $2\nu+\delta$, $2\nu-$

353   δ, Clark and Franks 1975; Pokrovski and Dubrovinski 2011; Pokrovski and Dubessy 2012) are

354   too weak and/or (partially) hidden by the more intense quartz peaks to be detectable in the

355   inclusions. Similarly, the third Raman active vibrational mode of S_3^-, the S-S asymmetric stretch

356   at ~580 cm^{-1}, was not detected because of its low intensity in the Raman resonance spectrum

357   dominated by the S-S stretch symmetric vibration (Chivers and Elders 2013; references therein).

358   The S-S stretch vibration of the S_3^- ion appears at 200°C as a high-frequency shoulder on

359   the large quartz band at ~464 cm^{-1} and grows, together with its corresponding overtones, with

360   increasing temperature in the three systems (Fig. 5a-5c). The formation of S_3^- is found to be rapid

361   and fully reversible with temperature changes. On heating, the intensity of the S_3^- bands stabilizes

362   within a few minutes following the T rise and remains constant during at least several hours at a

363   given T. Cooling the inclusion below 300-200°C results in almost instantaneous disappearance of

364   S_3^- and quantitative return to the sulfate-sulfide spectrum (Fig. 6). These findings strongly

365   suggest that S_3^- is not a short-lived transient complex that forms during a certain step in redox

366   reactions between sulfide, sulfate, and sulfur, but it is rather a product of thermodynamic

367   equilibrium among these sulfur species.

368   The effect of the laser beam power on the S_3^- formation was checked in the three systems.

369   Spectra on the same inclusions acquired with a laser power reduced by a factor of 2 to 10 were

370   identical to those obtained at full laser power, when normalized to the water band

16

Manuscript #4524R, Revision 1

371   (Supplementary Fig. 3). These results demonstrate that the lasers used in this study neither induce

372   the S_3^- formation through photochemical reactions, nor locally heat the inclusion which would

373   have increased the S_3^- abundance. Note that the laser wavelength affects significantly the S_3^-

374   Raman intensity, which is roughly 50% higher when acquired using the 637.7 nm (red) laser

375   compared to that of the 532.1 nm (green) laser, if H_2O is used as internal standard

376   (Supplementary Fig. 4). This is in agreement with the maximum absorbance of the S_3^- blue

377   chromophore ion at 610-620 nm, which favors a resonance phenomenon with the red laser having

378   a wavelength closer to this maximum (Clark and Franks 1975).

379

380   **DISCUSSION**

381   **Comparison with published data**

382   Our results show that S_3^- is stable in the aqueous liquid and supercritical fluid phases

383   containing ~3 wt% of total dissolved sulfur as sulfate and sulfide, at T from 200-300 to at least

384   500°C and P to ~1 kbar. The systematic growth of the normalized area of the S_3^- main Raman

385   peak in this temperature range in the three studied systems (Fig. 7) suggests that this species is

386   likely to be also stable at higher temperatures corresponding to the inclusion entrapment (600-

387   700°C). Accurate quantification of S_3^- amounts is not possible in the present study due to a)

388   intrinsic limitations of Raman spectroscopy applied to fluid inclusions (e.g., Roedder 1984;

389   Wopenka and Pasteris 1986; Pasteris et al. 1988), b) the presence of numerous intense bands of

390   quartz hiding the less intense peaks of dissolved sulfur species, and c) the absence of adequate

391   standards for the different sulfur species that must be measured in similar fluid inclusions

392   prepared under identical conditions to be comparable with the experimental samples.

393   Nevertheless, a very rough estimation of S_3^- concentrations may be tempting by comparing the

17

394   normalized areas of the S_3^- main peak ($A_{S_3^-}$) from this study (Fig. 7, Supplementary Table 2) with

395   those recently obtained on similar thiosulfate solutions in silica-glass capillary cells by Pokrovski

396   and Dubessy (2012) who used different calibration solutions of sulfate and sulfide to quantify the

397   S_3^- concentration. Comparison of the $A_{S_3^-}$ values of the present work ($A_{S_3^-}$ ~ 0.5-1.0 in 0.5 m

398    $K_2S_2O_3$ solutions at 400-500°C, Fig. 7) with those of their study ($A_{S_3^-}$ ~1.5-3.0 in a 1 m $K_2S_2O_3$

399   solution at similar T-P in which S_3^- attains ~0.3 m total S, Pokrovski and Dubessy 2012) suggests

400   that S_3^- accounts for at least 0.1 m (~ 0.3 wt%) of dissolved sulfur in the Thios and Thios-HCl

401   experiment.

402   Although S_3^- has been reported by chemists since 1970s in a variety of different media

403   such as non-aqueous solvents (Chivers and Drummond 1972; Clark and Cobbold 1978; Chivers

404   and Lau 1982), salt melts (Giggenbach 1971), silicate and borate glasses (Winther et al. 1998),

405   pigment minerals (Clark and Cobbold 1978; Reinen and Lindner 1999), and alkali metal-sulfur

406   butteries (Chivers and Elder 2013), little information is available about S_3^- in aqueous solution. A

407   blue color was observed ~100 years ago when sulfur was heated in water with traces of basic

408   salts (see Chivers 1974 and Chivers and Elder 2013 for overviews of old studies), followed much

409   later by UV-visible spectroscopy measurements on aqueous polysulfide solutions to 260°C

410   performed by Giggenbach (1971) who suggested the formation of another hypersulfide ion, S_2^-.

411   However, it is now admitted, on the basis of numerous spectroscopic and computational studies

412   of S_3^- in different media since mid-1970 (Chivers 1974; Steudel 2003, Chivers and Alder 2013;

413   references therein), that the blue color is due to S_3^-. Batch-reactor studies of sulfur speciation in

414   S-rich high-T aqueous solutions similar to those of this study did not detect S_3^- (Dadze and

415   Sorokin 1993; Pokrovski et al. 2008) likely because of its rapid breakdown to sulfate, sulfide, and

416   sulfur during solution sampling. Recent in situ studies of sulfur by Raman spectroscopy at high

Manuscript #4524R, Revision 1

417   *T-P* focused on the sulfate system at oxidizing conditions (Schmidt 2009; Ni and Keppler 2012).

418   Such conditions are thermodynamically unfavorable for S_3^- formation, which requires presence of

419   both oxidized and reduced sulfur forms. Only three in situ Raman spectroscopy studies at redox

420   conditions potentially favorable for S_3^- formation (sulfate-sulfide coexistence) have been

421   published so far. Bondarenko and Gorbaty (1997) investigated the S-H_2O system to 500°C and 1

422   kbar and reported intense Raman bands at 520-540 and 1060-1090 cm^{-1} that match very well the

423   S_3^- stretching vibration and its second overtone, but tentatively attributed these bands to other

424   species (SO_3 and/or $S_2O_5^{2-}$). Yuan et al. (2013) examined the S-H_2O-CH_4-D_2O system to ~400°C

425   and 1 kbar in short (< 0.7 h) heating runs, and found at some temperatures, together with H_2S,

426   HSO_4^- and SO_2, intense bands around 500 and 1400 cm^{-1}, which were not identified in their

427   study. The former band might be due to S_3^-, but acidic conditions and presumably low S

428   concentrations in their experiments might render its formation unfavorable. Pokrovski and

429   Dubrovinsky (2011) showed that S_3^- is stable above 250°C in solutions similar to those of this

430   study but at much higher pressures (5-50 kbar). The increasing stability of S_3^- at elevated *T-P* was

431   further confirmed by theoretical quantum-chemistry modeling (Tossell 2012).

432

433   **Implications**

434   This study and the recent findings discussed above clearly show that S_3^- forms at high

435   temperatures in S-rich aqueous systems (~few wt% S) containing sulfate, sulfide, and elemental

436   sulfur. The latter three S redox forms are commonly found in natural fluid (Rosasco and Roedder

437   1979; Bény et al. 1982; Boiron et al. 1999; Giuliani et al. 2003) and melt (Klimm and

438   Botcharnikov 2010) inclusions from different geological contexts. It is thus very likely that the

439   entrapped original fluids (and probably melts) in such systems contained S_3^- at elevated *T-P*.

440   However, the majority of Raman studies on such inclusions have been conducted at near-ambient

19

441   conditions, where S_3^- is not stable. The detection of S_3^- in such samples thus requires their heating

442   close to entrapment conditions, which may be technically challenging. Another complication of

443   sulfur speciation analyses in quartz-hosted natural fluid inclusions arises from post-entrapment

444   modifications, such as loss of hydrogen by diffusion (Bodnar 2003; Bakker 2009; references

445   therein) and gain of copper and probably other components (e.g., Lerchbaumer and Audétat

446   2012). These processes significantly and irreversibly alter the original fluid composition, pH, and

447   redox state. Thus, potential detection of S_3^- and other intermediate redox sulfur forms originally

448   present in high-temperature fluids and melts from natural inclusions is strongly conditioned by

449   the inclusion's post-entrapment evolution. Nevertheless, the findings of this study should

450   encourage people working on natural fluid and melt inclusions to perform Raman analyses at

451   elevated temperatures to estimate more reliably the sulfur speciation, at least in inclusions that

452   did not 'suffered' too much from their post-entrapment history.

453   The results of the present work in fluid inclusions, together with preliminary data of

454   Pokrovski and Dubessy (2012) in silica-glass capillary cells, extend the pressure range of the S_3^-

455   stability domain to conditions of S-rich magmatic-hydrothermal environments such as porphyry

456   systems hosting large part of economic gold, copper, and molybdenum resources. The chemical

457   similarity of S_3^- to regular polysulfides S_nS^{2-}, which are known to have strong bonding affinities

458   for soft metals like Au or Cu (Pokrovski et al. 2009), suggests that S_3^- is capable of forming

459   stable complexes with such metals. This was recently qualitatively confirmed by quantum-

460   chemical calculations of Cu-S_3 and Au-S_3 complexes (Tossell 2012; Mei et al. 2013). The S_3^- ion

461   may thus be a major carrier of chalcophile metals in fluids from porphyry systems, as initially

462   hypothesized by Pokrovski and Dubrovinsky (2011); however, experimental data on the stability

463   constants of S_3^- itself and metal-S_3^- complexes are required to make quantitative predictions of

464   metal transport. The fluids investigated in this study contained dissolved gold supplied by the Au

465   capsules. Work is currently in progress to determine Au concentrations in synthetic inclusions by

466   LA-ICP-MS and to correlate such analyses with the in situ sulfur speciation reported here in

467   order to quantify the role of S_3^- in Au transport at conditions of magmatic-hydrothermal gold

468   deposits.

469

470   **Acknowledgments**

474

21

Manuscript #4524R, Revision 1

475   **REFERENCES CITED**

476   Bakker, R. J. (2009) Reequilibration of fluid inclusions: Bulk diffusion. Lithos, 112, 277-288.

477   Banks, D.A. and Yardley, B.W.D. (1992) Crush-leach analysis of fluid inclusions in small natural

478   and synthetic samples. Geochimica et Cosmochimica Acta, 56, 245-248.

479   Barnes, H.L. (1979) Solubilities of Ore Minerals. In H.L. Barnes, Ed., Geochemistry of

480   hydrothermal ore deposits, p. 404-454. Wiley-Interscience, New York.

481   Bény, C., Guilhaumou, N., and Touray, J.-C. (1982) Native-sulphur-bearing fluid inclusions in

482   the CO_2-H_2S-H_2O-S system - Microthermometry and Raman microprobe (MOLE)

483   analysis - Thermochemical interpretations. Chemical Geology, 37, 113-127.

484   Binder, B. and Keppler, H. (2011) The oxidation state of sulfur in magmatic fluids. Earth and

485   Planetary Sciences Letters, 301, 190-198.

486   Bodnar, R.J. (2003) Re-equilibration of fluid inclusions. In I. Samson, A. Anderson and D.

487   Marshall, Eds., Fluid Inclusions: Analysis and Interpretation, 32, p. 213-231. Short

488   Course Series, Mineralogical Association of Canada, Vancouver, British Columbia.

489   Boiron, M.-C., Moissette, A., Cathelineau, M., Banks, D., Monnin, C., and Dubessy, J. (1999)

490   Detailed determination of palaeofluid chemistry: an integrated study of sulphate-

491   volatile rich brines and aquo-carbonic fluids in quartz veins from Ouro Fino (Brazil).

492   Chemical Geology, 154, 179-192.

493   Bondarenko, G.V. and Gorbaty, Y.E. (1997) In situ Raman spectroscopic study of sulfur-

494   saturated water at 1000 bar between 200 and 500 °C. Geochimica et Cosmochimica

495   Acta, 61, 1413-1420.

496   Bray, C.J. and Spooner, E.T.C. (1992) Fluid inclusion volatile analysis by gas-chromatography

497   with photoionization micro-thermal conductivity detectors - application to magmatic

498   MoS_2 and other H_2O-CO_2 and H_2O-CH_4 fluids. Geochimica et Cosmochimica Acta, 56,

499   261-272.

500   Burke, E.A.J. (2001) Raman microspectrometry of fluid inclusions. Lithos, 55, 139-158.

501   Catchpole, H., Kouzmanov, K., Fontboté, L., Guillong, M., and Heinrich, C.A. (2011) Fluid

502   evolution in zoned Cordilleran polymetallic veins - Insights from microthermometry

503   and LA-ICP-MS of fluid inclusions. Chemical Geology, 281, 293-304.

504   Catchpole, H., Kouzmanov, K., and Fontboté, L. (2012) Copper-excess stannoidite and

505   tennantite-tetrahedrite as proxies for hydrothermal fluid evolution in a zoned

506   Cordilleran base metal district, Morococha, central Peru. Canadian Mineralogist, 50,

507   719-743.

508   Cauzid, J., Philippot, P., Martinez-Criado, G., Menez, B., and Laboure, S. (2007) Contrasting Cu-

509   complexing behaviour in vapor and liquid fluid inclusions from the Yankee Lode tin

510   deposit, Mole Granite, Australia. Chemical Geology, 246, 39-54.

511   Chivers, T. (1974) Ubiquitous trisulfur radical ion S_3^-. Nature, 252 , 32-33.

512   Chivers, T. and Drummond, I. (1972) Characterization of the trisulfur radical anion S_3^- in blue

513   solutions of alkali polysulfides in hexamethylphosphoramide. Inorganic Chemistry, 11,

514   2525-2527.

515   Chivers, T. and Lau, C. (1982) Raman spectroscopic identification of the S_4N^- and S_3^- ions in

516   blue solutions of sulfur in liquid ammonia. Inorganic Chemistry, 21,453-455.

517   Chivers, T. and Elder, P.J.W (2013) Ubiquitous trisulfur radical ion: fundamentals and

518   applications in materials science, electrochemistry, analytical chemistry and

519   geochemistry. Chemical Society Reviews, 42, 5996-6005.

23

520   Clark, R.J.H and Cobbold, D.G. (1978) Characterization of sulfur radical anions in solutions of

521   alkali polysulfides in dimethylformamide and dexamethylphosphoramide and in the

522   solid state in ultramarine blue, green, and red. Inorganic Chemistry, 17, 3169-3174.

523   Clark, R.J.H. and Franks M.L. (1975) The resonance Raman spectrum of ultramarine blue.

524   Chemical Physics Letters, 34, 69-72.

525   Dadze, T.P. and Sorokin, V.I. (1993) Experimental determination of the concentrations of H_2S,

526   HSO_4^-, SO_{2aq}, $H_2S_2O_3$, S^0_{aq}, and S_{tot} in the aqueous phase in the $S-H_2O$ system at

527   elevated temperatures. Geochemistry International, 30, 38-53.

528   Driesner, T. and Heinrich, C.A. (2007) The system H_2O-NaCl. Part I: Correlation formulae for

529   phase relations in temperature-pressure-composition space from 0 to 1000 °C, 0 to

530   5000 bar, and 0 to 1 X_{NaCl}. Geochimica et Cosmochimica Acta ,71, 4880-4901.

531   Dubessy, J., Boiron, M.-C., Moissette, A., Monnin, C., and Sretenskaya, N. (1992)

532   Determinations of water, hydrates and pH in fluid inclusions by micro-Raman

533   spectrometry. European Journal of Mineralogy, 4, 885-894.

534   Dubessy, J., L'Homme, T., Boiron, M.-C., and Rull, F. (2002) Determination of chlorinity in

535   aqueous fluids using Raman spectroscopy of the stretching band of water at room

536   temperature: application to fluid inclusions. Applied Spectroscopy 56, 99-106.

537   Duc-Tin, Q., Audétat, A., and Keppler, H. (2007) Solubility of tin in (Cl, F)-bearing aqueous

538   fluids at 700 °C, 140 MPa: A LA-ICP-MS study on synthetic fluid inclusions.

539   Geochimica et Cosmochimica Acta, 71, 3323-3335.

540   Einaudi, M.T., Hedenquist, J.W., and Inan E.E. (2003) Sulfidation state of fluid in active and

541   extinct hydrothermal systems: transitions from porphyry to epithermal environments. In

542   S.F. Simmons and I. Graham, Eds., Volcanic, Geothermal, and Ore-forming Fluids:

543   Rulers and Witnesses of Processes within the Earth. Society of Economic Geologists

544   Special Publication, 10, 285-313.

545   Frank, M.R., Simon, A.C., Pettke, T., Candela, P.A., and Piccoli, P.M. (2011) Gold and copper

546   partitioning in magmatic-hydrothermal systems at 800 °C and 100 MPa. Geochimica et

547   Cosmochimica Acta, 75, 2470-2482.

548   Frantz, J.D., Dubessy, J., and Mysen, B. (1993) An optical cell for Raman spectroscopic studies

549   of supercritical fluids and its application to the study of water to 500 °C and 2000 bar.

550   Chemical Geology, 106, 9-26.

551   Frezzotti, M.L., Tecce, F., and Casagli, A. (2012) Raman spectroscopy for fluid inclusion

552   analysis. Journal of Geochemical Exploration, 112, 1-20.

553   Gibert, F., Guillaume, D., and Laporte, D. (1998) Importance of fluid immiscibility in the H_2O-

554    $NaCl$-CO_2 system and selective CO_2 entrapment in granulites: experimental phase

555   diagram at 5-7 kbar, 900 °C and wetting textures. European Journal of Mineralogy, 10,

556   1109-1123.

557   Giggenbach, W. (1971) The blue solutions of sulfur in water at elevated temperatures. Inorganic

558   Chemistry, 10, 1306-1308.

559   Giuliani, G., Dubessy, J., Banks, D., Vinh, H.Q., Lhomme, T., Pironon, J., Garnier, V., Trinh,

560   V.T., Long, P.V., Ohnenstetter, D., and Schwarz, D. (2003) CO_2-H_2S-COS-S_8-

561    $AlO(OH)$-bearing fluid inclusions in ruby from marble-hosted deposits in Luc Yen

562   area, North Vietnam. Chemical Geology, 194, 167-185.

563   Goldstein, R.H. and Reynolds, T.J. (1994) Systematics of fluid inclusions in diagenetic minerals.

564   Society for Sedimentary Geology short course 31, Tulsa, Oklahoma.

Manuscript #4524R, Revision 1

565   Guillong, M., Latkoczy, C., Seo, J.H., Günther, D., and Heinrich, C.A. (2008) Determination of

566   sulfur in fluid inclusions by laser ablation ICP-MS. Journal of Analytical Atomic

567   Spectrometry, 23, 1581-1589.

568   Hedenquist, J.W. and Lowenstern, J.B. (1994) The role of magmas in the formation of

569   hydrothermal ore deposits. Nature, 370, 519-527.

570   Helgeson, H.C., Kirkham, D.H., and Flowers, G.C. (1981) Theoretical prediction of the

571   thermodynamic behavior of aqueous electrolytes at high pressures and temperatures:

572   IV. Calculation of activity coefficients, osmotic coefficients and apparent molal and

573   relative partial molal properties to 600° C and 5 kb. American Journal of Science, 281,

574   1249-1516.

575   Jacquemet, N., Pironon, J., and Caroli, E. (2005) A new experimental procedure for simulation of

576           $H_2S + CO_2$ geological storage - Application to well cement aging. Oil & Gas Science

577   and Technology - Rev. IFP, 60, 193-206.

578   Jacquemet, N., Pironon, J., Lagneau, V., and Saint-Marc, J. (2012) Armouring of well cement in

579   H_2S-CO_2 saturated brine by calcite coating - Experiments and numerical modeling.

580   Applied Geochemistry, 27, 782-795.

581   Johnson, J.W., Oelkers, E.H. and Helgeson, H.C. (1992) SUPCRT92: A software package for

582   calculating the standard molal thermodynamic properties of minerals, gases, aqueous

583   species, and reactions from 1 to 5000 bar and 0 to 1000 °C. Computers & Geosciences,

584   18, 899-947, available at http://geopig.asu.edu/?q=tools.

585   Klimm, K. and Botcharnikov, R.E. (2010) The determination of sulfate and sulfide species in

586   hydrous silicate glasses using Raman spectroscopy. American Mineralogist, 95, 1574-

587   1579.

26

588   Kouzmanov, K. and Pokrovski, G.S. (2012) Hydrothermal controls on metal distribution in Cu(-

589   Au-Mo) porphyry systems. In J.W. Hedenquist, M. Harris, and F. Camus, Eds.,

590   Geology and Genesis of Major Copper Deposits and Districts of the World: A Tribute

591   to Richard H. Sillitoe. Society of Economic Geologists Special Publication, 16, 573-

592   618.

593   Lamb, W.M., Popp, R.K., and Boockoff, L.A. (1996) The determination of phase relations in the

594   CH_4-H_2O-NaCl system at 1 kbar, 400 to 600 °C using synthetic fluid inclusions.

595   Geochimica et Cosmochimica Acta, 60, 1885-1897.

596   Lerchbaumer, L. and Audétat, A. (2012) High Cu concentrations in vapor-type fluid inclusions:

597   An artifact? Geochimica et Cosmochimica Acta, 88, 255-274.

598   Mei Y., Sherman D.M., Liu W., and Brugger J. (2013) Complexation of gold in S_3^--rich

599   hydrothermal fluids: Evidence from ab-initio molecular dynamics simulations.

600   Chemical Geology, 347, 34-42.

601   Meyer, B., Ospina, M., and Peter, L.B. (1980) Raman spectrometric determination of oxysulfur

602   anions in aqueous systems. Analytica Chimica Acta, 117, 301-311.

603   Meyer, B., Ward, K., Koshlap, K., and Peter, L. (1983) Second dissociation constant of hydrogen

604   sulfide. Inorganic Chemistry, 22, 2345-2346.

605   Mullis, J., Dubessy, J., Poty, B., and O'Neil, J. (1994) Fluid regimes during late stages of a

606   continental collision: Physical, chemical, and stable isotope measurements of fluid

607   inclusions in fissure quartz from a geotraverse through the Central Alps, Switzerland.

608   Geochimica et Cosmochimica Acta, 58, 2239-2267.

609   Ni, H. and Keppler, H. (2012) In-situ Raman spectroscopic study of sulfur speciation in oxidized

610   magmatic-hydrothermal fluids. American Mineralogist, 97, 1348-1353.

611   Oelkers, E.H., Bénézeth, P., and Pokrovski, G.S. (2009) Thermodynamic Databases for Water-

612   Rock Interaction. In E.H. Oelkers and J. Schott, Eds, Thermodynamics and Kinetics of

613   Water-Rock Interaction, 70, p. 1-46. Reviews in Mineralogy & Geochemistry,

614   Mineralogical Society of America, Chantilly, Virginia.

615   Ohmoto, H., and Lasaga, A.C. (1982) Kinetics of reactions between aqueous sulfates and sulfides

616   in hydrothermal systems. Geochimica et Cosmochimica Acta, 46, 1727-1745.

617   Pasteris, J.D., Wopenka, B., and Seitz, J.C. (1988) Practical aspects of quantitative laser Raman

618   microprobe spectroscopy for the study of fluid inclusions. Geochimica et

619   Cosmochimica Acta, 52, 979-988.

620   Pasteris, J.D., Freeman, J.J., Goffredi, S.K., and Buck, K.R. (2001) Raman spectroscopic and

621   laser scanning confocal microscopic analysis of sulfur in living sulfur-precipitating

622   marine bacteria. Chemical Geology, 180, 3-18.

623   Pironon, J., Jacquemet, N., Lhomme, T., and Teinturier, S. (2007) Fluid inclusions as micro-

624   samplers in batch experiments: A study of the system C-O-H-S-cement for the potential

625   geological storage of industrial acid gas. Chemical Geology, 237, 264-273.

626   Pokrovski, G.S. and Dubessy, J. (2012) In situ Raman spectroscopy reveals new sulfur forms in

627   high-temperature geological fluids. In Proceedings of the 10th International Conference

628   on Raman Spectroscopy applied to Earth Sciences - sensu lato (Georaman X[th]), p. 77-

629   78, Nancy, France.

630   Pokrovski, G.S. and Dubrovinsky, L.S. (2011) The S_3^- ion is stable in geological fluids at

631   elevated temperatures and pressures. Science, 331, 1052-1054.

632   Pokrovski, G.S., Borisova, A.Y., and Harrichoury, J.-C. (2008) The effect of sulfur on vapor-

633   liquid fractionation of metals in hydrothermal systems. Earth and Planetary Science

634   Letters, 266, 345-362.

28

Manuscript #4524R, Revision 1

635   Pokrovski, G.S., Tagirov, B.R., Schott, J., Hazemann, J.-L., and Proux, O. (2009) A new view on

636   gold speciation in sulfur-bearing hydrothermal fluids from in situ X-ray absorption

637   spectroscopy and quantum-chemical modeling. Geochimica et Cosmochimica Acta, 73,

638   2506-2527.

639   Poty, B. and Stalder, H.A. (1974) Fluid inclusions studies in quartz from fissures of Western and

640   Central Alps. Schweizerische Mineralogische und Petrographische Mitteilungen, 54,

641   717–752.

642   Pryor, W.A. (1960) The kinetics of the disproportionation of sodium thiosulfate to sodium sulfide

643   and sulfate. Journal of the American Chemical Society, 82, 4794-4797.

644   Reinen, D. and Lindner, G.-G. (1999) The nature of the chalcogen colour centres in ultramarine-

645   type solids. Chemical Society Reviews, 28, 75-84.

646   Rudolph, W. (1996) Structure and dissociation of the hydrogen sulfate ion in aqueous solution

647   over a broad temperature range: a Raman study. Zeitschrift für Physikalische Chemie,

648   194, 73-95.

649   Roedder, E. (1984) Nondestructive methods of determination of inclusion composition. In P.H.

650   Ribbe, Ed., Fluid inclusions, 12, p 79-108. Reviews in Mineralogy, Mineralogical

651   Society of America, Washington D.C..

652   Rosasco, G.J. and Roedder, E. (1979) Application of a new Raman microprobe spectrometer to

653   nondestructive analysis of sulfate and other ions in individual phases in fluid inclusions

654   in minerals. Geochimica et Cosmochimica Acta, 43, 1907-1915.

655   Ryan, C.G., Heinrich, C.A., and Mernagh, T.P. (1993) PIXE microanalysis of fluid inclusions

656   and its application to study ore metal segregation between magmatic brine and vapor.

657   Nuclear Instruments and Methods in Physics Research Section B, 77, 463-471.

658   Schmidt, C. (2009) Raman spectroscopic study of a $H_2O + Na_2SO_4$ solution at 21-600 °C and 0.1

659   MPa to 1.1 GPa: Relative differential ν_1-SO_4^{2-} Raman scattering cross sections and

660   evidence of the liquid–liquid transition. Geochimica et Cosmochimica Acta, 73, 425-

661   437.

662   Seo, J.H., Guillong, M., and Heinrich, C.A. (2009) The role of sulfur in the formation of

663   magmatic-hydrothermal copper-gold deposits. Earth and Planetary Science Letters,

664   282, 323-328.

665   Seo, J.H., Guillong, M., and Heinrich, C.A. (2012) Separation of molybdenum and copper in

666   porphyry deposits: The roles of sulfur, redox, and pH in ore mineral deposition at

667   Bingham Canyon. Economic Geology, 107, 333-356.

668   Seward, T.M. and Barnes, H.L. (1997) Metal transport by hydrothermal ore fluids. In H.L.

669   Barnes, Ed., Geochemistry of hydrothermal ore deposits, p. 435-486. John Wiley &

670   Sons, New York.

671   Shapiro, S.M., O'Shea, D.C., and Cummins, H.Z. (1967) Raman scattering study of the alpha-

672   beta transition in quartz. Physical Review Letters, 19, 361-364.

673   Shvarov, Y.V. (2008) HCh: New potentialities for the thermodynamic simulation of geochemical

674   systems offered by Windows. Geochemistry International, 46, 834-839.

675   Sillitoe, R.H. (2010) Porphyry copper systems. Economic Geology, 105, 3-41.

676   Simon, A.C. and Ripley, E.M. (2011) The role of magmatic sulfur in the formation of ore

677   deposits. In H. Behrens and J.D. Webster, Eds., Sulfur in Magmas and Melts: Its

678   Importance for Natural and Technical Processes. Reviews in Mineralogy and

679   Geochemistry, 73, 513-578.

30

Manuscript #4524R, Revision 1

680 Sterner, S.M. and Bodnar, R.J. (1984) Synthetic fluid inclusions in natural quartz I.

681 Compositional types synthesized and applications to experimental geochemistry.

682 Geochimica et Cosmochimica Acta, 48, 2659-2668.

683 Steudel, R. (2003) Elemental Sulfur and Sulfur-rich Compounds II, 248 p. Springer, Berlin.

684 Tossell, J.A. (2012) Calculation of the properties of the S_3^- radical anion and its complexes with

685 Cu^+ in aqueous solution. Geochimica et Cosmochimica Acta, 95, 79-92.

686 Tsujimura, T., Xuea, X., Kanzakia, M., and Waltera, M.J. (2004) Sulfur speciation and network

687 structural changes in sodium silicate glasses: Constraints from NMR and Raman

688 spectroscopy. Geochimica et Cosmochimica Acta, 68, 5081-5101.

689 Ulrich, T. and Mavrogenes, J. (2008) An experimental study of the solubility of molybdenum in

690 H_2O and $KCl-H_2O$ from 500 °C to 800 °C, and 150 to 300 MPa. Geochimica et

691 Cosmochimica Acta, 72, 2316-2330.

692 Uyama, F., Chiba, H., Kusakabe, M. and Sakai, H. (1985) Sulfur isotope exchange reactions in

693 the aqueous system: thiosulfate-sulfide-sulfate at hydrothermal temperature.

694 Geochemical Journal, 19, 301-315.

695 Winther, K.T., Watson, E.B., and Korenowski, G. (1998) Magmatic sulfur compounds and sulfur

696 diffusion in albite melt at 1 GPa and 1300-1500 °C. American Mineralogist, 83, 1141-

697 1151.

698 Wojdyr, M. (2010) Fityk: a general-purpose peak fitting program. Journal of Applied

699 Crystallography, 43, 1126-1128.

700 Wopenka, B. and Pasteris, J.D. (1986) Limitations to quantitative analysis of fluid inclusions in

701 geological samples by laser Raman microprobe spectroscopy. Applied Spectroscopy,

702 40, 144-151.

31

Manuscript #4524R, Revision 1

703   Yuan, S., Chou, I-M., Burruss, R.C., Wang, X., and Li, J. (2013) Disproportionation and

704   thermochemical sulfate reduction reactions in $S-H_2O-CH_4$ and $S-D_2O-CH_4$ systems

705   from 200 to 340°C at elevated pressures. Geochimica et Cosmochimica Acta, 118, 263-

706   275.

707   Zajacz, Z., Seo, J.H., Candela, P.A., Piccoli, P.M., Heinrich, C.A., and Guillong, M. (2010)

708   Alkali metals control the release of gold from volatile-rich magmas. Earth and

709   Planetary Science Letters, 297, 50-56.

710   Zajacz, Z., Seo, J.H., Candela, P.A., Piccoli, P.M., Heinrich, C.A., and Tossell, J.A. (2011) The

711   solubility of copper in high-temperature magmatic vapors: A quest for the significance

712   of various chloride and sulfide complexes. Geochimica et Cosmochimica Acta, 75,

713   2811-2827.

714   Zhang, L., Audétat, A., and Dolejŝ, D. (2012) Solubility of molybdenite (MoS_2) in aqueous fluids

715   at 600-800 °C, 200 MPa: a synthetic fluid inclusion study. Geochimica et

716   Cosmochimica Acta, 77, 175-185.

717

Manuscript #4524R, Revision 1

718   **Table 1**. Chemical compositions and temperature and pressure conditions of fluid inclusion

719   synthesis and Raman measurements.

Experiment	Composition	T (°C), P (bar) of fluid inclusion entrapment	T (°C), P (bar) of Raman measurements
Thios	0.45 m $K_2S_2O_3$ + 0.05 m $Na_2S_2O_3$	600, 2000	25, P_{sat}* 200, P_{sat} 300, P_{sat} 400, 500†
Thios-HCl	0.42 m $K_2S_2O_3$ + 0.04 m $Na_2S_2O_3$ + 0.51 m HCl	600, 2000	25, P_{sat} 200, P_{sat} 300, P_{sat} 400, 500†
S-NaOH	1.01 m S + 0.37 m NaOH	700, 2000	25, P_{sat} 200, P_{sat} 300, P_{sat} 400, 400† 500, 900†

720

721   Notes: m designates molinity (number of moles of solute per one kg of solution).

722   * P_{sat} = saturated vapor pressure in the two-phase liquid-vapor system, which is approximated by

723   the H_2O-NaCl-H_2S system, using the PVTX properties of the NaCl-H_2O system from Driesner

724   and Heinrich (2007), H_2S vapor-liquid partitioning coefficients from Johnson et al. (1992), the

725   sulfur liquid-phase speciation from Figure 1, and approximate mass balance of sulfur between the

726   vapor and liquid phase. These estimations indicate that P_{sat} values in the synthesized fluid

727   inclusions are ~1, 20, and 90 (±10-20%) bar at 25, 200, and 300°C, respectively.

728   † pressure is determined using the isochores in Fig. 2.

729
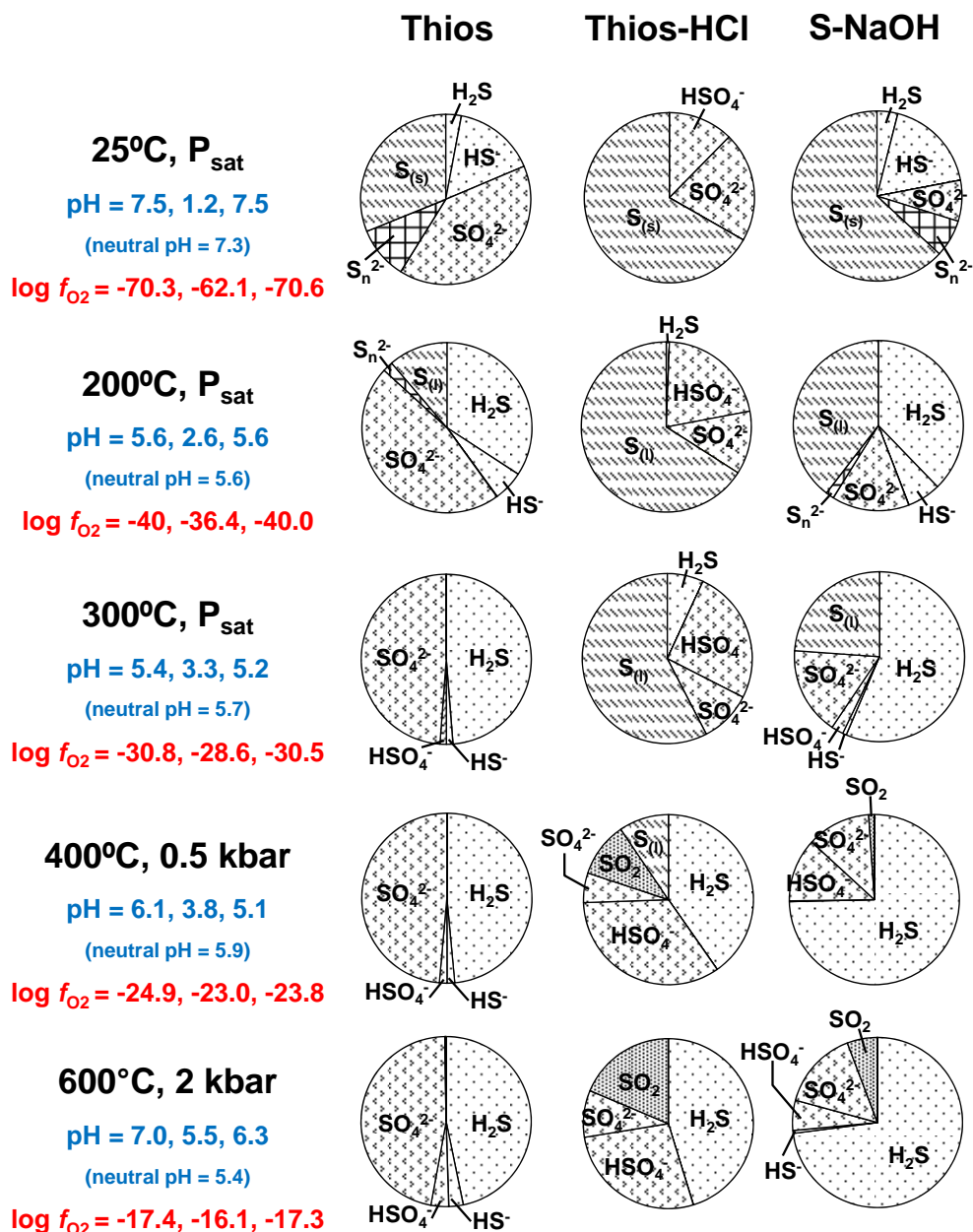
Figure 1. Calculated sulfur species distribution, pH, and oxygen fugacity (f_{O2} in bar) at different *T-P* conditions in the three systems, using thermodynamic properties of sulfur species available in the literature (see Supplementary Table 1). The fraction of SO_4^{2-} stands for the sum of SO_4^{2-} and its ion pairs $NaSO_4^-$ and KSO_4^-; HSO_4^- stands for the sum of HSO_4^- and its ion pairs $KHSO_4^0$ and $NaHSO_4^0$; minor sulfur species (< 1% of total dissolved sulfur) are not shown for clarity.

34

Manuscript #4524R, Revision 1

737
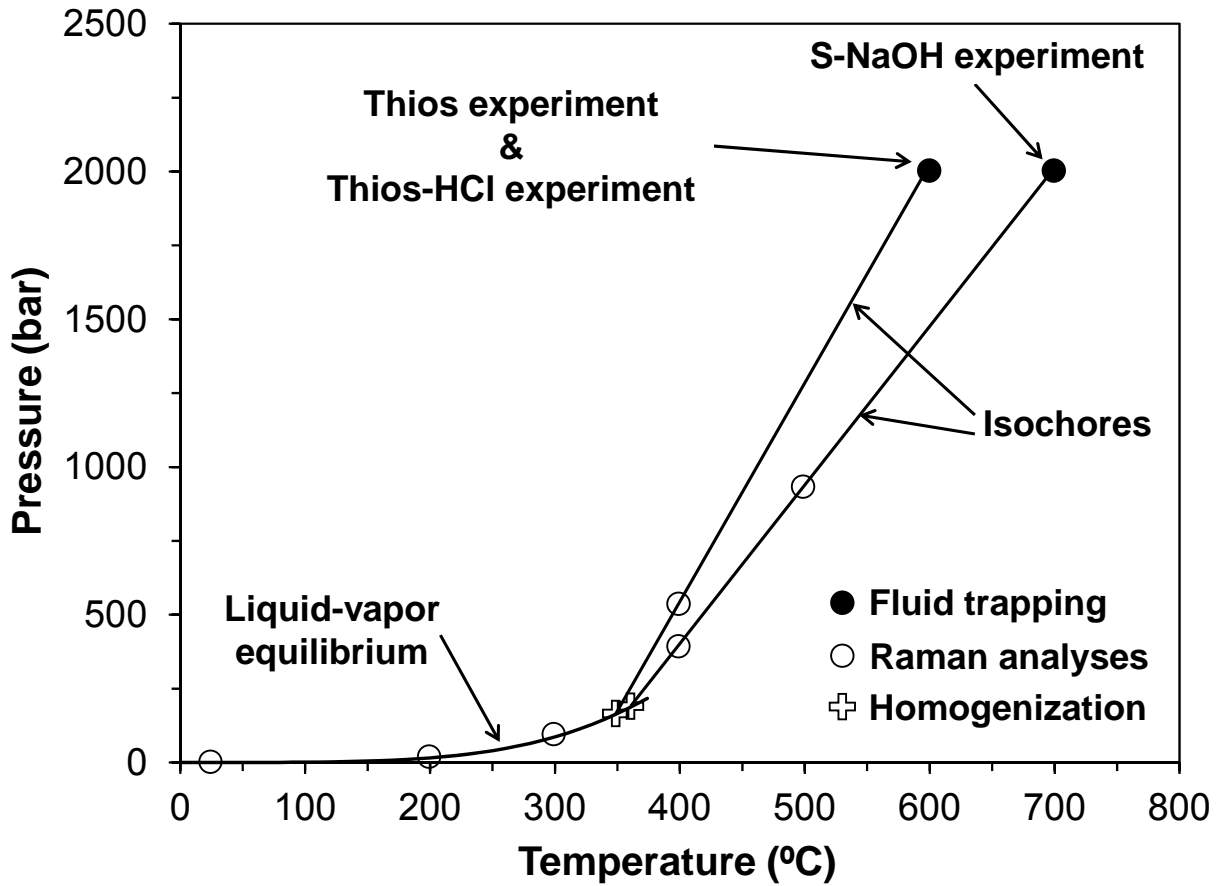
Figure 2. Pressure-temperature conditions of the fluid inclusion synthesis and Raman spectroscopy analyses.

738

739

740
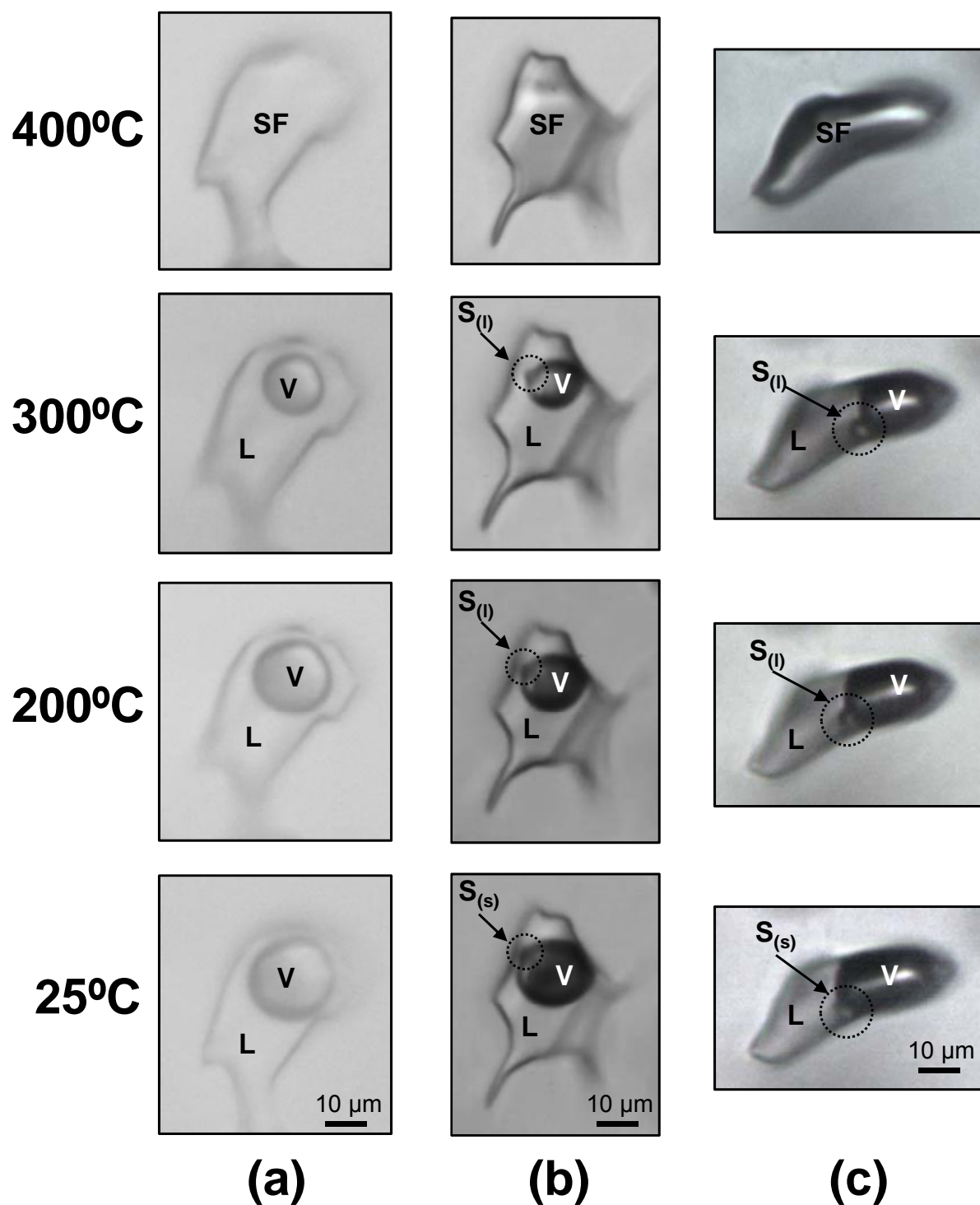
Figure 3. Fluid inclusion microphotographs obtained during microthermometry measurements in the Thios (a), Thios-HCl (b), and S-NaOH (c) systems. L: liquid, V: vapor, SF: supercritical fluid, $S_{(s)}$: solid elemental sulfur, $S_{(l)}$: molten elemental sulfur.

36

744
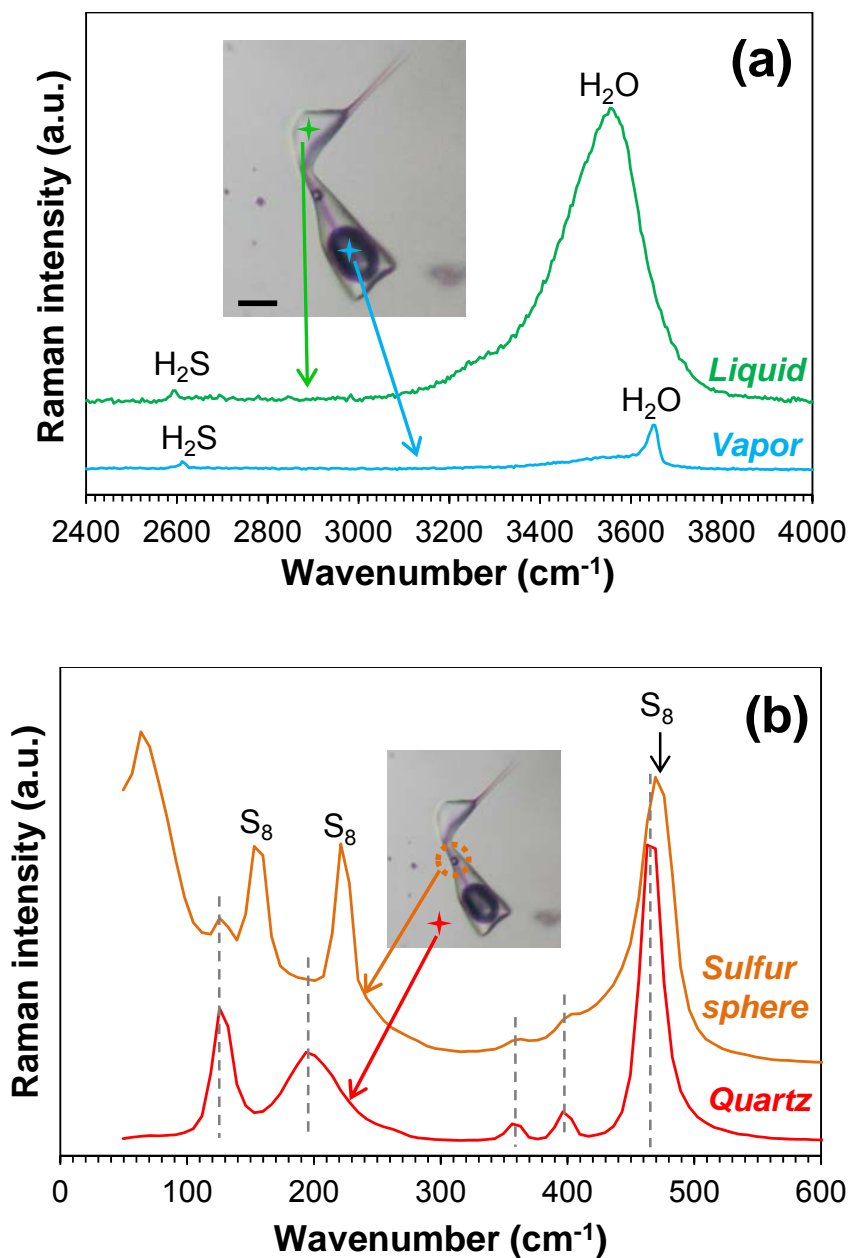
Figure 4. Raman spectra of aqueous liquid and vapor at 300°C (a) and molten sulfur at

300°C (b) in a representative fluid inclusion from the Thios-HCl experiment. The laser spots on

the different phases are shown by crosses. A Raman spectrum of quartz recorded in the proximity

of the fluid inclusion is also shown in panel b; the vertical dashed lines indicate the quartz peaks

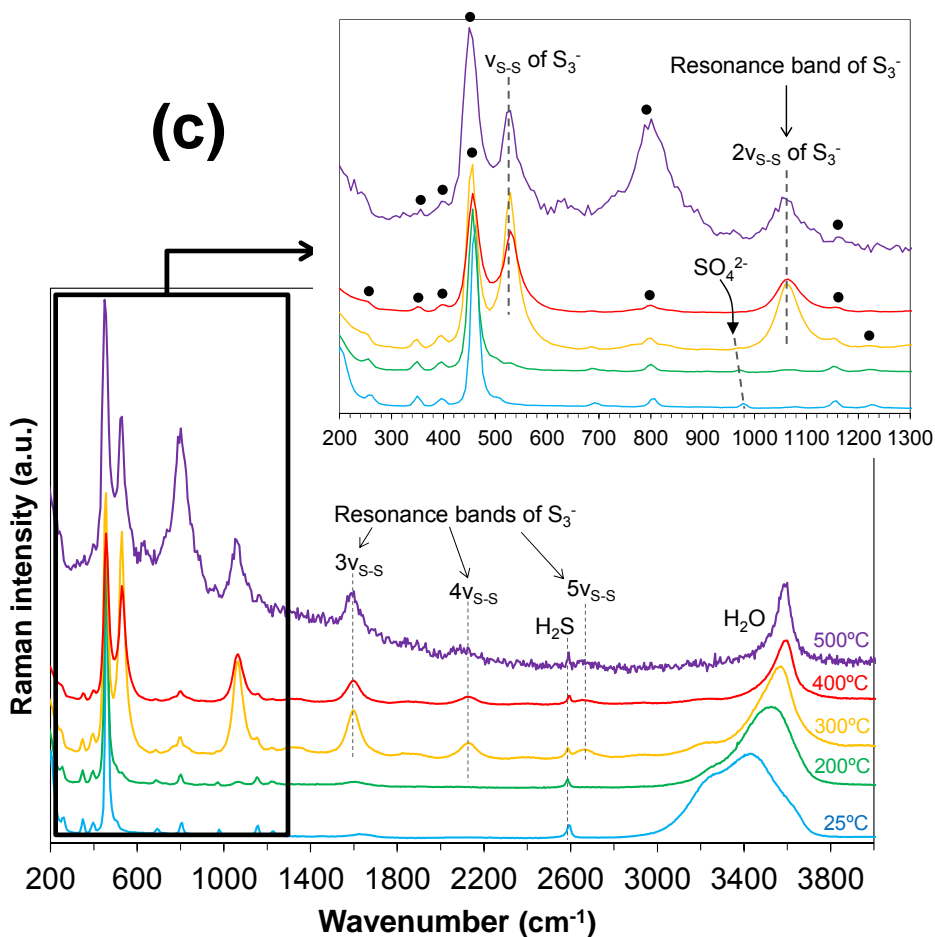positions. The Raman frequencies of molten sulfur (153, 221, and 469 cm^{-1}) correspond to those

of the S$_8$ molecular polymorph (Pasteris et al. 2001; Giuliani et al. 2003; Frezzotti et al. 2012).

37

Manuscript #4524R, Revision 1

751

752

Manuscript #4524R, Revision 1
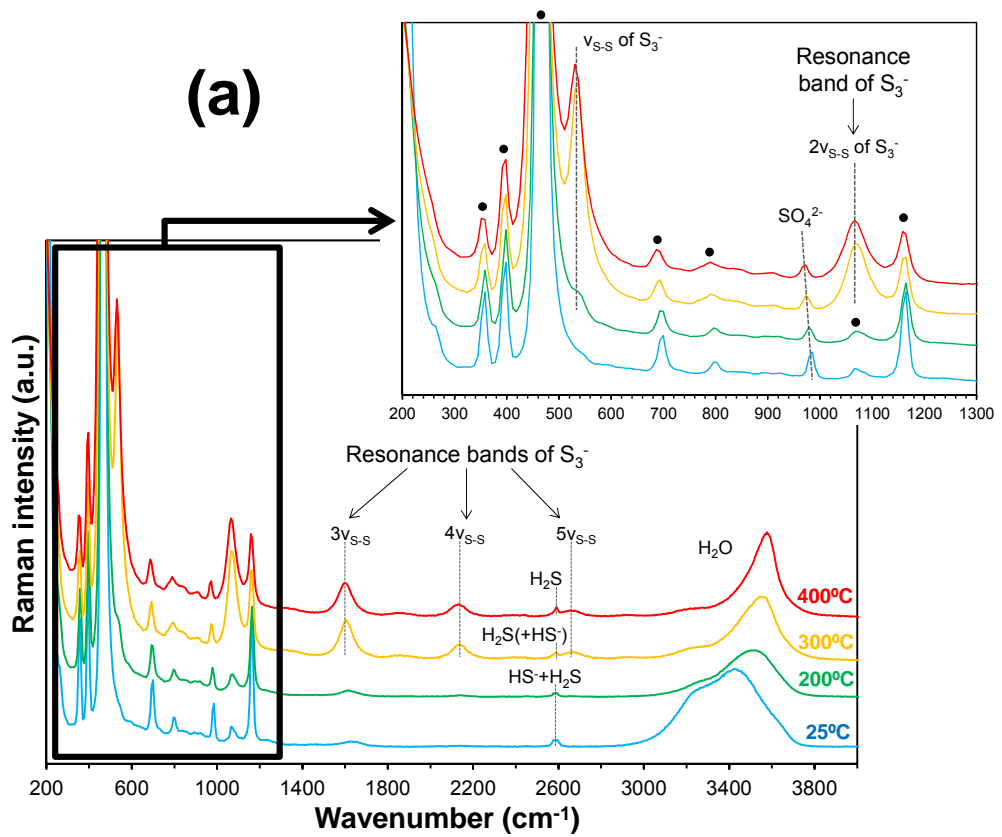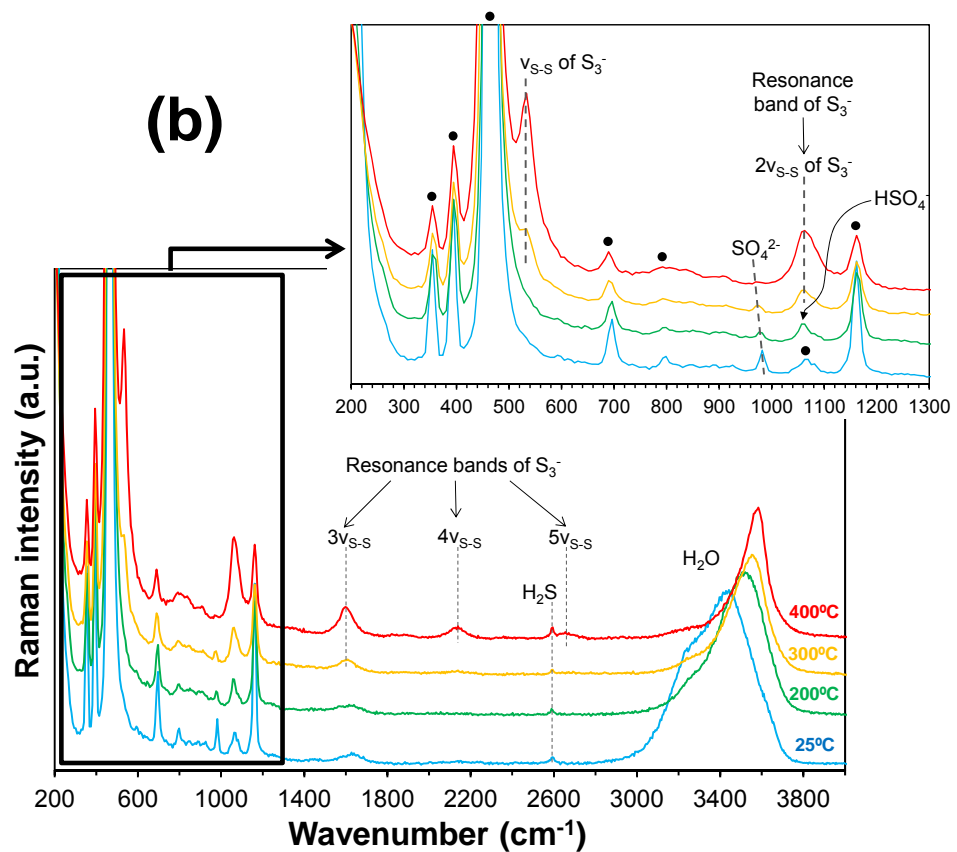
Figure 5. Raman spectra of the aqueous liquid and supercritical phase in synthesized fluid inclusions, obtained from the Thios (a), Thios-HCl (b), and S-NaOH (c) systems at the indicated temperatures. The spectra are normalized to 12, 20, and 60 seconds of acquisition in the three systems, respectively, and are offset vertically. The black dots indicate the quartz peaks. At 500°C in the S-NaOH system, the spectra acquisition is affected by quartz surface disordering near the α–β quartz transition that may be induced by the laser beam spot, resulting in noisier spectra, peak broadening and intensity increase of the 800 cm^{-1} peak belonging to β-quartz.

761
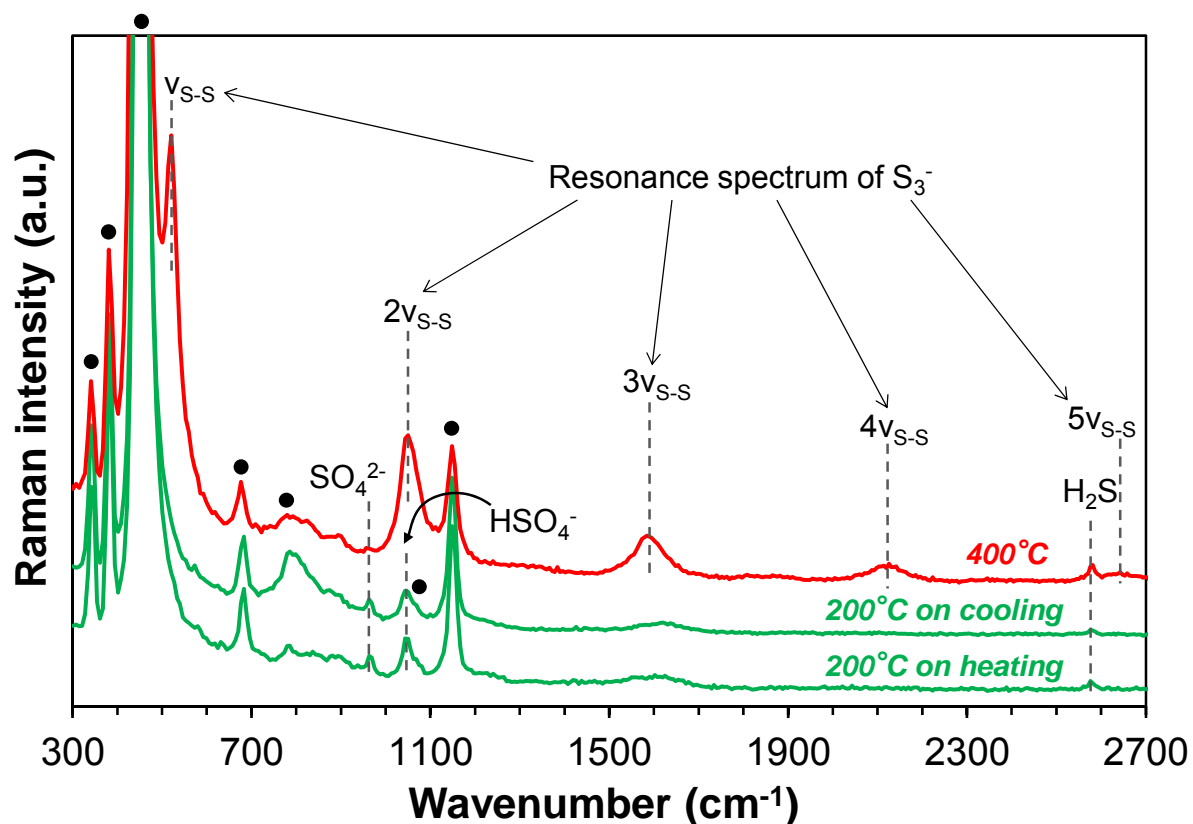
Figure 6. Raman spectra of the aqueous liquid phase at 200°C obtained on heating to and cooling from 400°C in the Thios-HCl experiment. The spectra are normalized to 15 seconds of acquisition time and offset vertically. The black dots indicate the quartz peaks. The quartz peak at ~800 cm^{-1} obtained at 200°C on cooling is broadened and enhanced due to quartz disordering/phase transition as also observed in the S-NaOH experiment at higher temperature (Fig. 5c).

40

768
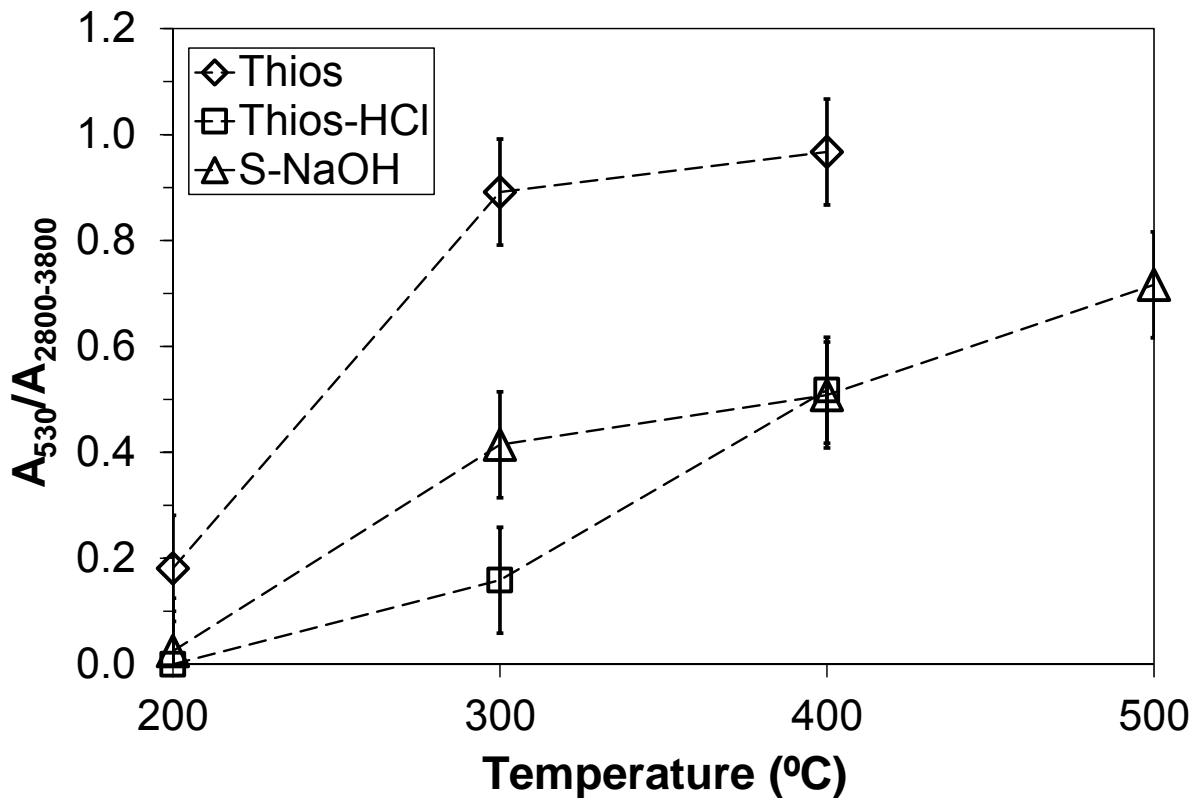
Figure 7. Normalized integrated intensity of the S_3^- main Raman peak ($A_{530}/A_{2800-3800}$, where A_{530} and $A_{2800-3800}$ stand, respectively, for the areas of the S-S stretching vibration of S_3^- at ~530 cm^{-1} and O-H stretching vibrations of H_2O between 2800 and 3800 cm^{-1}) acquired with the 532 nm laser in the aqueous liquid and supercritical fluid phase in the three systems as a function of temperature.